

Effect of Ultrasound on the Austenite Transformation of Shape Memory Alloys

Ali H. Alhilfi

University of Misan, Baghdad road R4QR+5R8, 62001, Maysan, Iraq
alihameed@stud.uni-obuda.hu

Endre Ruzinkó

Óbuda University, Népszínház St. 8, H-1081 Budapest, Hungary
ruszinko.endre@uni-obuda.hu

Abstract: The paper aims to develop a model describing the shape memory deformation in the presence of ultrasonic impulses. The application of ultrasound can be of great importance, primarily when heating the shape memory alloy elements cannot be carried out for many applications. Experimental results record that acoustic waves induce the austenitic transformation, which manifests itself in a jump-wise increment in the deformation as ultrasound is On. The model presented here is constructed in terms of the synthetic theory of irrecoverable deformation. To catch the phenomena caused by acoustic energy, we enter into the basic equation a new term reflecting the effect of ultrasound on the processes governing the phase transformation. The analytical results fit good experimental data.

Keywords: shape memory alloys; austenitic transformation; ultrasound

1 Introduction

Today Shape Memory Alloys (SMAs) are already commercially applied in many technical fields. SMAs have been developed since the early 1960s, and since then, they have been successfully used for medical [1, 2, 3], robotic [4, 5, 6], aerospace [7, 8, 9], and automobile applications [10, 11].

The superior property of SMA is that it can go through solid-state phase transformations, meaning it can be stretched, bent, heated, cooled, and still remember its original shape. SMAs are widely used for medical implants in medicine due to their kink resistance, stress constancy, high elasticity, and corrosion resistance. If we speak of electronic devices and robotic systems, SMA

actuators, sensors, and controllers have drawn significant attention and interest due to their unique properties and are expected to be equipped in many modern vehicles at competitive market prices [12]. The essential advantage is that active elements (e.g., SMA wire or spring) can be deformed by applying minimal external force and retain their previous form when subjected to certain stimuli such as thermomechanical or magnetic changes. In aerospace, SMA release devices can be actuated slowly, avoiding satellite shock failures. This application is essential for satellites because it can also be used for 'microsatellites' since compact separation devices with minimal SMA release triggers can be made [13].

As mentioned above, SMAs show a particular ability to recuperate the original shape while heating above specific critical temperatures (shape memory effect). In other words, they can recover a large unelastic deformation or create high recovery stress on heating within the temperature range of martensitic transformation. However, heating the shape memory alloy elements cannot be carried out for many applications. Other ways to initiate shape memory effects may be applied in these cases. It is known that strain recovery may be initiated by neutron irradiation, hydrostatic pressure, and ultrasonic action [14]. The last method is the most attractive because ultrasonic vibration does not require expensive equipment like other methods.

This paper concentrates our attention on the effect of ultrasonic vibrations on the shape memory effect (austenitic transformation on heating). Experimental observations on this topic [15, 16, 17, 18, 19, 20] can be summarised as follows (Fig. 1):

- I. Ultrasonic vibrations impulsively added to austenitic transformation on heating result in negative strain jumps. In other words, acoustic energy can initiate strain variations of SMA.
- II. The magnitude of the strain jumps increases with the ultrasonic vibration amplitude.
- III. The effect of insonation strongly depends on the moment when the ultrasound is applied. Acoustic energy results in no effect if it acts outside the austenite transformation temperature range, i.e., before A_s or after A_f . Further, the magnitude of the ultrasound-induced strain jumps is not distributed uniformly within the austenite transformation temperature range. This phenomenon reaches its maximum if the alternate stresses are applied approximately in the middle of the temperature range of phase transformations. It can be explained by the fact that the action of ultrasound manifests itself in full force when the amount of material involved in transformation is maximum. The lattice is very soft during transformation, and the phase boundaries are very movable. In this case, any external action, for instance, alternate stress, results in the appearance of an additional quantity of preferably oriented

domains, which leads to a further strain variation. The number of phase boundaries reaches its maximum when half of the alloy is transformed into the austenite phase [14].

- IV. It was found that the series of ultrasonic impulses led to the finish temperature being less than during conventional heating. Since acoustic energy boosts the transformation processes, it is logical to assume that they sooner reach their completeness. In other words, the temperature needed to finish the transformation is partially compensated by ultrasound heating.
- V. After switching of ultrasound, the further realization of SME is observed according to the reverse transformation kinetics. However, immediately after the ultrasound is off, some "backsliding" in austenitic deformation, a slight increase of deformation, is observed; 67-77°C temperature range in Fig. 1. This aftereffect is assumed to be due to a) the decrease in temperature after ultrasound is off and b) the action of ultrasound which "left a trail" in the form of ultrasound-assisted defect conglomeration, reducing the development of the phase transformations. Therefore, while the central portion of acoustic energy converts irreversibly into the phase deformation increment, some fraction of it recovers.

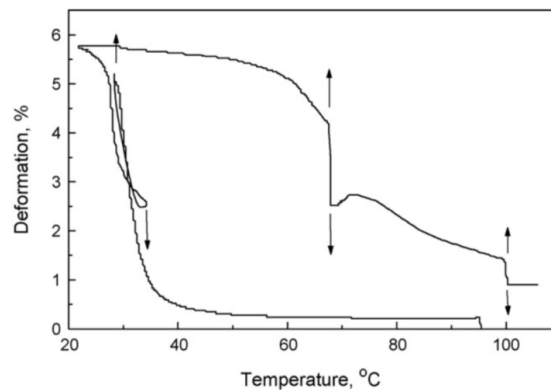


Figure 1

State diagram of NiTi alloy in deformation-temperature coordinate. The sample is subjected to uniaxial tension $\sigma = 30$ MPa. The arrows show the moments of switching-on (\uparrow) and switching-off (\downarrow) of ultrasonic vibrations [16].

Experimental papers clearly show that stress and temperature are equal stimuli for initiating martensite/austenite transformations, i.e., the same mechanical effects can be achieved by employing both stress and temperature. Since ultrasound is a carrier of both these effects – alternating stress and increase in temperature caused by them – the physical substantiation of the phenomena observed above can be summarised as follows [14, 15, 16, 17, 18, 19, 20]:

- I. The variation (increase) in austenite deformation can be explained by ultrasonic heating of the sample due to ultrasound waves' energy dissipation and the formation of steady austenite.
- II. Acoustic energy increases the mobility of interfaces (phase and domains) by decreasing the efficient friction force caused by alternate stresses.
- III. The superposition of alternate stresses induces the movement of interface and martensitic domain boundaries (within the temperature range of reverse martensitic transformations).
- IV. The lattice is very soft during transformation, and the phase boundaries are very movable. In this case, any external action, for instance, alternate stress, results in the appearance of an additional quantity of preferably oriented domains, which leads to a further strain variation. The number of phase boundaries reaches its maximum when half of the alloy is transformed into the austenite phase.

This paper aims to develop a model describing analytically the austenitic transformation of NiTi alloy subjected to ultrasound impulses. For the mathematical apparatus, we take the synthetic theory of irrecoverable deformation, which has established itself as a reliable instrument to model many problems in the field of phase transformation [21, 22, 23].

2 Synthetic Theory

The synthetic theory operates with notions used in the Ilyushin deviatoric space, such as stress and strain vector, \mathbf{S} and \mathbf{e} [23]. For a three-dimensional subspace (\mathbf{S}^3) of the Ilyushin five-dimensional deviatoric space, we have

$$\begin{aligned}
 S_1 &= \sqrt{3/2}S_{xx}, S_2 = S_{xx} / \sqrt{2} + \sqrt{2}S_{yy}, S_3 = \sqrt{2}S_{xz} \\
 e_1 &= \sqrt{3/2}e_{xx}, e_2 = e_{xx} / \sqrt{2} + \sqrt{2}e_{yy}, e_3 = \sqrt{2}e_{xz}
 \end{aligned} \tag{1}$$

where S_{ij} and e_{ij} are the stress and strain deviator tensor components, respectively. As a two-level model, the synthetic theory calculates the macroscopic deformation as an averaging (summation) of deformations occurring on the micro level of material. For the macro level, we take the elementary volume of the body, which is considered a point in the mathematical sense. This volume consists of a large number of micro volumes, each being an element of the continuum capable of deforming under external effects. Thus, macrodeformation is defined as the integration (summation) of deformations occurring on the microscopic level of material. As a result, we propose the following formula for strain vector components (e_k) [23]

$$e_k = \iiint_V \varphi_N N_k dV, \quad k = 1, 2, 3. \quad (2)$$

The formula above is derived for such stress states when $\mathbf{S} \in \mathbf{S}^3$. In Eq. (2), φ_N is named strain intensity; it is an average measure of deformation within one microstructure element. N_k are components of unit vector (\mathbf{N}) giving the orientation of this element, which are defined via spherical angles α , β , and λ in. The range of angles α , β , and λ is $0 \leq \alpha \leq 2\pi$, $0 \leq \beta \leq \pi/2$, and $0 \leq \lambda \leq \pi/2$ [23]. In terms of the Synthetic theory, the development of inelastic deformation is derived via planes in \mathbf{S}^3 , their positions are defined through angles α , β , and λ as shown in Fig. 2 [23].

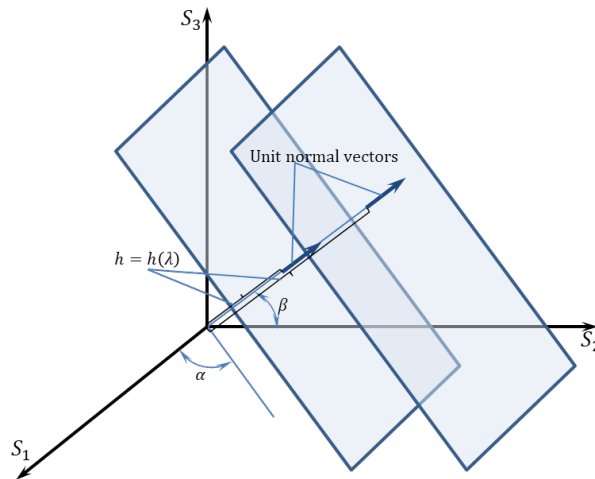


Figure 2

Locations of planes in \mathbf{S}^3 given by angles α and β , and the plane distance $h(\lambda)$

Finally, dV from (2) is an elementary set of micro volumes involved in the deformation [23]

$$dV = \cos \beta d\alpha d\beta. \quad (3)$$

Now, we have to define the strain intensity. To apply Eq. (2) to the description of deformations induced by phase transformations, we relate the strain intensity rate to the rate of martensite fraction ($\dot{\Phi}$) [23]:

$$r\dot{\varphi}_N = \dot{\Phi}, \quad (4)$$

where r is the model constant. We define $\dot{\Phi}$ as [23]

$$\dot{\Phi} = -\frac{\dot{T}_e}{M_s - M_f}, \quad (5)$$

where \dot{T}_e is the rate of effective temperature, which will be defined below. This formula holds for martensitic transformation at

$$\dot{T}_e < 0 \text{ and } M_f < T_e < M_s. \quad (6)$$

For austenitic transformation, we write [23]

$$\dot{\Phi} = -\frac{\dot{T}_e}{A_f - A_s}, \dot{T}_e > 0 \text{ and } A_s < T_e < A_f \quad (7)$$

Formulae (5)-(7) give a linear relationship between the martensite fraction and effective temperature, which is widely accepted in the scientific community (Fig. 3).

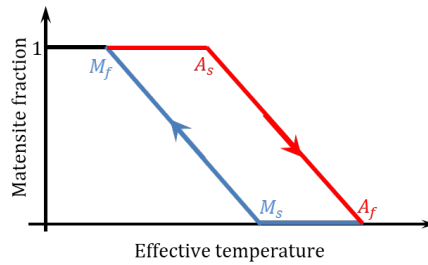


Fig. 3

$\Phi \square T_e$ graph plotted via Eqs. (5)-(7)

In Eq. (7), T_e is effective temperature proposed in terms of the structural-analytic model by [24], through the Clausius-Clapeyron equation, as [23]

$$T_e = T(1 - DS \cdot \mathbf{N}), \quad (8)$$

where D is the model constant. Formula (8) determines the start/finish temperatures as a function of temperature and acting stress [23, 24]. Fig. 4 demonstrates the change in effective temperature from (8) for differently orientated elements (for simplicity, we set $\lambda = 0$). As one can see, the start and finish of the transformation strongly depend on the orientation of the element we consider.

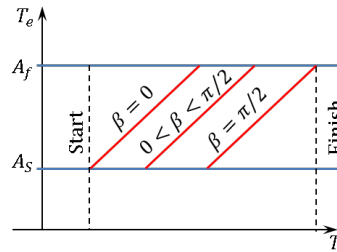


Figure 4

Effective temperature for different directions ($S = \text{const}$)

Eq. (8) enables one to account for the shift of the characteristic temperatures caused by loading. Summarising, formulae (5)-(8) define the amount of martensite as a single-valued function of temperature and acting load. The scalar product $\mathbf{S} \cdot \mathbf{N}$ gives the resolved shear stress acting in the element with \mathbf{N} -orientation. This fact reflects the well-known fact that external load manifests itself differently depending on how preferable the element's/slip system's orientation is.

With Eqs. (4), (7), and (8), φ_N for austenitic transformation is

$$r\dot{\varphi}_N = \dot{\Phi} = -\frac{\dot{T}_e}{A_f - A_s}, \quad (9)$$

Differentiating in (8), we get

$$r\dot{\varphi}_N = -\dot{T}_e = -\dot{T}(1 - DS \cdot \mathbf{N}) + TD\dot{\mathbf{S}} \cdot \mathbf{N}. \quad (10)$$

In the formula above, the constant r includes $A_f - A_s$.

Consider austenitic transformation on heating when the material is under the action of constant stress, $\dot{\mathbf{S}} = 0$. Eq. (10) gives

$$r\dot{\varphi}_N = -\dot{T}(1 - DS \cdot \mathbf{N}) \quad (11)$$

Let us apply the above formula for the case of uniaxial tension when the stress vector, according to (1), has only one non-zero component, $S_1 = \sqrt{2/3}\sigma \equiv S$, and, together with (3), we have [23]

$$r\dot{\varphi}_N = -\dot{T}(1 - DS_1 N_1) = -\dot{T}(1 - DS \sin \beta \cos \lambda). \quad (12)$$

On integrating in (12), we have

$$r\varphi_N = -T(1 - DS \sin \beta \cos \lambda) + C \quad (13)$$

The integration constant C is determined from the condition that the austenite transformation terminates ($\varphi_N = 0$) as the effective temperature reaches the

austenite finish temperature, A_f . Since the transformation completion takes place at $\beta = \pi/2$ and $\lambda = 0$, we can calculate the austenitic transformation finish temperature, T_f . Equating T_e from (8) for the specified angle values to A_f , we obtain $T_f = A_f / (1 - DS)$. Now, Eq. (13) at $\varphi_N = 0$, $T = T_f$, $\beta = \pi/2$, and $\lambda = 0$ gives $C = A_f$. So

$$r\varphi_N = -(T - A_f) + TDS \sin \beta \cos \lambda. \quad (14)$$

Fig. 5 schematically shows the $\varphi_N \sim T$ graphs plotted with Eq. (14) for different values of β . Again, it is easy to see that different elements are involved in the transformation for different temperature ranges. Fig. 6 demonstrates the $\varphi_N \sim \beta$ graphs plotted with Eq. (14) for different effective temperatures. As one can see, at the start of martensitic transformation, when the material is in a martensitic state ($\Phi = 1$), φ_N takes positive values over the whole diapason of angle β (lines 1 and 2). As the temperature increases, the domain of angles β with positive strain intensities decreases and finally shrinks to the point $\beta = \pi/2$ where $\Phi = 0$). The boundary values of angles λ and β (points 1, 1', 1" for lines 3-5) are obtained from conditions $\varphi_N = 0$ and $\lambda = 0$

$$\cos \lambda_1 = \frac{1}{DS \sin \beta} \left(1 - \frac{A_f}{T} \right), \quad \sin \beta_1 = \frac{1}{DS} \left(1 - \frac{A_f}{T} \right). \quad (15)$$

Here we assume that $T > A_f$; for $T < A_f$ we let $\beta_1 = 0$ and $\lambda_1 = \pi/2$ (lines 1 and 2 in Fig. 6).

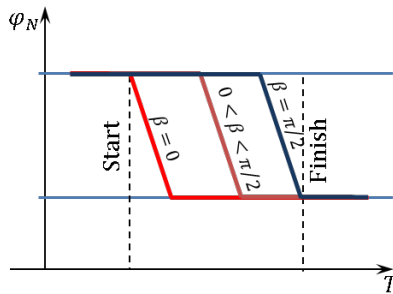


Figure 5
 $\varphi_N \sim T$ plots for different angles β ($\lambda = 0$, $S = \text{const}$).

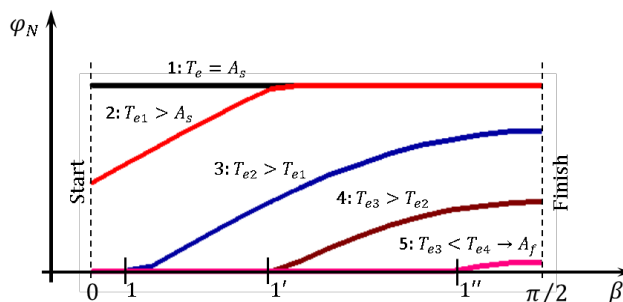


Figure 6

$\varphi_N \sim \beta$ plots for different effective temperatures ($\lambda = 0$, $S = \text{const}$)

Therefore, the initial stage of martensite-austenite transition is described by Eq. (2) with the integration diapason $0 \leq \alpha \leq 2\pi$, $0 \leq \beta \leq \pi/2$, and $0 \leq \lambda \leq \pi/2$ (lines 1 and 2 in Fig. 6), and in the course of temperature increase, when the domain of non-zero strain intensities shrinks (lines 3-5 in Fig. 6), the integral (2) becomes

$$e = \int_0^{2\pi} \int_0^{\pi/2} \int_0^{\beta_1} \varphi_N N_1 \cos \beta d\alpha d\beta d\lambda. \quad (16)$$

3 Extension of the Synthetic Theory to the Ultrasound-assisted Shape Memory Deformation

Since effective temperature is the most crucial factor in the progress of phase transformation – T_e directly influences the values of Φ and φ_N –, we propose to extend Eq. (8) by a term reflecting the presence of ultrasound. Following the observations on the effect of ultrasound on austenitic transformation, we propose to shift (increase) the value of effective temperature by a term (U) representing the ultrasound action:

$$T_e = T(1 - DS \cdot \mathbf{N}) + U. \quad (17)$$

We decompose the U on two components to reflect the thermal and the mechanical impact of acoustic energy on the kinetics of the austenitic transformation.

$$U = f(S_U) \cdot g(T). \quad (18)$$

The first term points out the assisting action of ultrasound due to the generation of alternating stresses that induce and intensify the movement of interface and martensitic domain boundaries. We define $f(S_U)$ as

$$f(S_U) = \left(B + e^{-w(T-T_i)} \right) \int_{A_s}^T U_1(\mathbf{S}_U \cdot \mathbf{N}) dt, \quad (19)$$

where T_i are the temperatures as ultrasound is On; U_1 , w , and B are model constants and \mathbf{S}_U is a stress vector whose components are formed via Eq. (1) by the values of alternating stress amplitudes. Considering short-termed ultrasound impulses, f is assumed to increase in a jump-wise manner as the ultrasound is On. Then, it decreases, stabilizing at some value after the ultrasound is Off. The overall effect of the ultrasonic impulses is an increase in f . Although $\mathbf{S}_U = 0$ between the ultrasound impulses, $f(S_U) > 0$ throughout the transformation due to the integration in (19) that cumulates positive values during the sonication.

We propose the term $U_1(\mathbf{S}_U \cdot \mathbf{N})$ in (19) to comply with experimental data stating that the magnitude of the strain jumps is proportional to stress amplitudes (\mathbf{S}_U), and the effectiveness of ultrasound varies depending on the orientation of the microregion considered. It is the scalar product $\mathbf{S}_U \cdot \mathbf{N}$ that reflects the effectiveness of the ultrasound action for a given orientation. The presence of $\left(B + e^{-w(T-T_i)} \right)$ in (19) reflects the experimental fact that after ultrasound is Off, the so-called aftereffect is recorded, consisting of some deformation increase. As $e^{-w(T-T_i)} \rightarrow 0$, the further realization of SME takes place according to the austenite transformation kinetics, although shifted by B . To summarize, the effect of ultrasound manifests itself in the recoverable and irrecoverable portions of phase deformation.

In order to catch the experimental observation recording that the strain-jump magnitude strongly depends on the temperature when ultrasound is applied, we propose the function $g(T)$ from (18) in the form of the Agnesi curve:

$$g(T) = \frac{a^3}{a^2 + (T - C)^2}. \quad (20)$$

While the function f leads to uniform strain increments at a given ultrasonic intensity, the function g gives different strain-jump magnitudes depending on the transformation stage when the acoustic energy acts. The model constants a and C from (20) reflect the material's compliance to react to the ultrasonic impact at different moments of the transformation.

Figure 7 demonstrates the $U(T)$ plot, which shows its step-wise increments at the temperatures as the ultrasound is On. The magnitudes of these increments vary with the temperature.

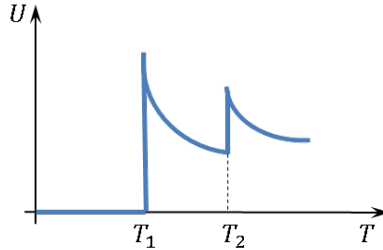


Figure 7

Dependence of U on temperature; ultrasonic impulses are applied at $T = T_1$ and $T = T_2$

Consider the case when a material is fully austenitic ($\Phi = 0$) and subjected to the action of constant uniaxial stress. Let an impulse of longitudinal ultrasound at a given temperature be applied. In this case, the vector S_U , according to (1), has components $(\sqrt{2/3}\sigma_m, 0, 0)$, where σ_m is the amplitude of oscillating tension-compression stress.

Now, the strain intensity, on the base of Eqs. 14 and (17)-(20), is

$$r\varphi_{NU} = -(T - A_f) + (TDS - U)\sin\beta\cos\lambda. \quad (21)$$

The shape memory deformation (e_u), according to Eq. (2), takes the following form (the integral over α gives 2π)

$$e_u = \frac{\pi}{r} \int_0^{\lambda_{1U}} \int_{\beta_{1U}}^{\pi/2} \left[-(T - A_f) + (TDS - U)\sin\beta\cos\lambda \right] \sin 2\beta \cos \lambda d\lambda d\beta \quad (22)$$

The boundary angles in (22) are

$$\cos \lambda_{1U} = \frac{1}{(DS - U)\sin\beta} \left(1 - \frac{A_f}{T} \right), \quad \sin \beta_{1U} = \frac{1}{(DS - U)} \left(1 - \frac{A_f}{T} \right). \quad (23)$$

Like in Eq. (15), we assume that $T > A_f$, otherwise, we let $\beta_{1U} = 0$ and $\lambda_{1U} = \pi/2$.

Figure 8 gives a comparison between $\varphi_{NU} \sim T$ and $\varphi_N \sim T$ plots, which demonstrate entire agreement with experimental observations:

Ultrasound induces the deformation recovery on heating, i.e., intensifies the shape memory deformation. This is due to the term U in Eq. (21) reflecting the promoting action of ultrasound within microelements. In an instant as ultrasound On, the deformation yields a negative increment and, after a short disturbance, follows the kinetics of austenitic transformation. Another effect from U is that the amount of material involved in the transformation increases due to ultrasonic impulse, i.e., by comparing (15) and (23), we have $\lambda_{1U} < \lambda_1$ and $\beta_{1U} > \beta_1$. Besides, formula (20) governs the magnitude of the strain jump depending on the temperature of ultrasonic insonation. Summing the strain intensities in all the micro volumes taking part in the austenitic transformation, Eq. (22), we obtain the deformation on the macroscopic scale.

Since acoustic energy boosts the phase transformation, it ends at less temperature than the ordinary shape memory effect – in Fig. 8, the φ_{NU} line reaches sooner than φ_N the zero value.

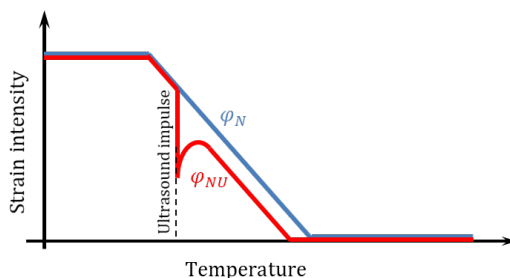


Figure 8

Strain intensity vs. temperature for an ordinary (φ_N) case and with ultrasound (φ_{NU})

Therefore, the extension of the synthetic theory expressed in formulae (17)-(23) leads to a qualitative correspondence with experiments. The next step is to inspect its quantitative correctness.

4 Results. Discussion

Here, our goal is to plot $\varepsilon \sim T$ diagram of NiTi alloy at fixed static stress subjected to ultrasonic insonation and compare it with the experiment. Characteristic temperatures of the alloy measured by differential scanning calorimetry were: $A_s = 323$ K, $A_f = 349$ K [16]. The procedure of tests was the following. The wire sample in the high-temperature austenite was subjected to load (uniaxial tension $\sigma = 30$ MPa that results in deformation of 1.9%) with subsequent cooling. After cooling, the sample was brought into austenitic condition by heating. The heating was performed at a rate of 1 K/min.

Two ultrasonic impulses (each of 9 sec [14-16]) with vibrational amplitude $A = 5 \mu\text{m}$ and frequency $f = 22.2 \text{ kHz}$ were produced in the temperature range $A_s - A_f$. The first ultrasonic impulse was produced at $T_1 = 340 \text{ K}$ and the second at $T_2 = 373 \text{ K}$.

To calculate the alternating stress amplitudes σ_m , we utilize the following relationship

$$\sigma_m = E \frac{2\pi f}{c} A, \quad (24)$$

where E and c is the NiTi alloy's Young modulus and the speed of sound, respectively. Taking into account that these are temperature functions, further, we utilize their average values for $A_s - A_f$ diapason: $E = 62 \text{ GPa}$, $c = 5200 \text{ m/s}$ [25], [26]. As a result, from (24), we have $\sigma_m = 8.3 \text{ MPa}$.

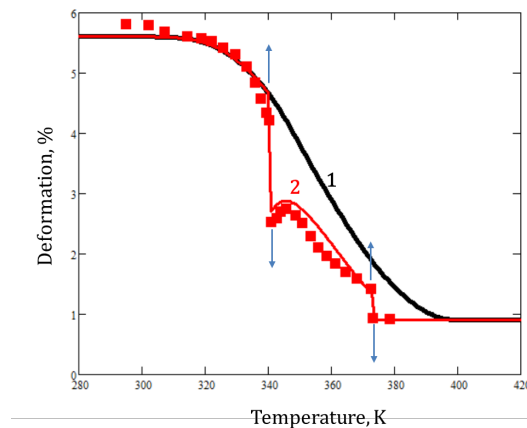


Figure 9

State diagram of NiTi alloy in deformation-temperature coordinate. The sample is subjected to uniaxial tension $\sigma = 30 \text{ MPa}$. The arrows show the moments of switching-on (\uparrow) and switching-off (\downarrow) of ultrasonic vibrations; ■ –experiment [16], lines – model.

First, we plot the $\varepsilon \sim T$ diagram for the shape memory effect with the above data without ultrasonic action. To do this, we use Eqs. (14)-(16) for plotting line 1 in Fig. 9 with the following model constants: $D = 4.2 \times 10^{-3} \text{ MPa}^{-1}$ and $r = 4.9 \times 10^2 \text{ K}$. At least for the temperature diapason 290-340 K, i.e., before the first ultrasonic impulse, we can conclude that the model curve shows good agreement with the experiment.

The next step is the $\varepsilon \sim T$ diagram in the presence of ultrasonic impulses (line 2 in Fig. 9). Formulae (17)-(23) give the value of strain jumps shown in Table 1. The model results have been obtained with the following values of constants: $w = 1.32 \times 10^{-1} \text{ K}^{-1}$, $U_1 = 13.83 (\text{K} \cdot \text{MPa})^{-1}$, $a = 4.0 \text{ K}$, $C = 360 \text{ K}$, $B = 4.79 \times 10^{-1}$. It must be stressed that the values of constants D and r stay the same as in the previous paragraph. The magnitude of the strain jump at the first impulse is much greater than that at the second. The reason is that the first impulse is done near the middle of the transformation while the second is closer to its end. The same result is obtained analytically because of the function $g(T)$ (20), where the constant C regulates the temperature of the greatest increment in the deformation caused by ultrasound. Therefore, the magnitude of strain jumps is governed by constants U_1 in $f(S_U)$ and a in $g(T)$, and the constant C in $g(T)$ regulates the temperature of the maximum ultrasound effect.

Table 1
Strain jumps due to ultrasound impulses

	Experiment	Model	Relative error, %
1st impulse	1.675	1.973	+15.1
2nd impulse	0.493	0.445	-9.7

The kinetics of $\varepsilon \sim T$ after switching off of ultrasound is also in full accordance with experimental results. Namely, after the strain jump, the model result shows some increase in the deformation, after which the deformation on heating develops according to the reverse transformation kinetics. This result is due to term $(B + e^{-w(T-T_i)})$ in $f(S_U)$. Here, constant w governs the duration of the deformation's increase following the ultrasonic action, and B expresses an irrecoverable portion of deformation caused by ultrasound. Thus, the model accounts for another experimental fact stating that the ultrasound-assisted transformation ends at lower temperatures. In our case, the second ultrasonic impulse results in such a drop in deformation that the material achieves a fully austenitic state when the further increase in temperature results in no deformation variation. So, we read from Fig. 9 that the finish temperature after two acoustic impulses is 373 K, while the ordinary $\varepsilon \sim T$ diagram stops its variation at about 400 K.

In summarizing, we may conclude that the extension of the synthetic theory leads to qualitatively and quantitatively correct results.

Conclusion

We developed a model that predicts the kinetics of ultrasound-assisted austenitic transformation. This model was created in terms of the synthetic theory of irrecoverable deformation. Following the results of experimental observations,

stating that the presence of ultrasounds affects/translates the transformation temperatures, we extended the formula for effective temperature by the term accounting for the presence of acoustic energy. As a result, we derived a formula to calculate deformations as a function of temperature at constant static stress under the action of ultrasonic impulses. The analytical results obtained are in full accordance with the experiment. Namely, (i) deformation yields a jump-wise increment at the instant as ultrasound is On; (ii) after ultrasound is Off, the deformation incurs some increase, after which strain-temperature diagram runs according to austenitic transformation kinetics, although beneath the standard curve; (iii) the magnitude of strain jump strongly depends on the temperature when the acoustic impulse is produced – as approaching the middle of the phase temperature range the jump tends to a maximum; (iv) the presence of acoustic energy results in the decrease of the finish temperature. Since the analytical results show good accuracy, the model presented in this paper can be treated as an effective instrument for describing ultrasound-assisted austenitic transformations.

References

- [1] Bansiddhi A, Sargeant T, Stupp S and Dunand D (2008) Porous nickel-titanium for bone implants: a review. *Acta Biomaterialia* 4, pp. 773-782
- [2] Morgan N (2004) Medical shape-memory alloy applications—the market and its products. *Materials Science and Engineering: A* 378(1-2): 16-23
- [3] Sun L, Huang WM, Ding Z et al. (2012) Stimulus-responsive shape-memory materials: a review. *Materials & Design* 33: 577-640
- [4] Kim B, Lee MG, Lee YP, Kim Y and Lee G (2006) An earthworm-like micro robot using shape-memory alloy actuator. *Sensors and Actuators A: Physical* 125(2): 429-437
- [5] Qin CJ, Ma PS and Yao Q (2004) A prototype micro-wheeled-robot using shape memory alloy actuator. *Sensors and Actuators A: Physical* 113(1): 94-99
- [6] Wang Z, Hang G, Li J, Wang Y and Xiao K (2008) A micro-robot fish with embedded shape-memory alloy wire actuated flexible biomimetic fin. *Sensors and Actuators A: Physical* 144(2): 354-360
- [7] Hartl D and Lagoudas DC (2007) Aerospace applications of shape-memory alloys. *Proceedings of the Institution of Mechanical Engineers, Part G: Journal of Aerospace Engineering* 221(4): 535-552
- [8] Hartl D, Lagoudas D, Calkins F and Mabe J (2010a) Use of a Ni60Ti shape memory alloy for active jet engine chevron application: I. Thermomechanical characterization. *Smart Materials and Structures* 19(1): 015020
- [9] Hartl D, Mooney J, Lagoudas D, Calkins F and Mabe J (2010b) Use of a Ni60Ti shape-memory alloy for active jet engine chevron application: ii.

- Experimentally validated numerical analysis. *Smart Materials and Structures* 19(1): 015021
- [10] Bellini A, Colli M and Dragoni E (2009) Mechatronic design of a shape memory alloy actuator for automotive tumble flaps: a case study. *IEEE Transactions on Industrial Electronics* 56(7): 2644-2656
- [11] Stoeckel D (1990) Shape-memory actuators for automotive applications. *Materials & Design* 11(6): 302-307
- [12] Jani, J. M., Leary, M., & Subic, A. (2014) Shape Memory Alloys in Automotive Applications. *Applied Mechanics and Materials*, 663, 248-253
- [13] Wanhill, R. J. H., & Ashok, B. (2017) Shape memory alloys (SMAs) for aerospace applications. *Aerospace Materials and Material Technologies*, 467-481
- [14] Belyaev, S., Volkov, A., & Resnina, N. (2014) Alternate stresses and temperature variation as factors of influence of ultrasonic vibration on mechanical and functional properties of shape memory alloys. *Ultrasonics*, 54(1), 84-89
- [15] Klubovich, V. V., Rubanik, V. V., Likhachev, V. A., Rubanik Jr., V. V. Dorodeiko, V. G. (1997) Generation of shape memory effect in Ti-Ni alloy by means of ultrasound, in A. Pelton, D. Hodgson, S. Russel, T. Duering (Eds.), *Proc of the 2nd International Conference on Shape Memory and Superelastic Technologies, SMST*, pp. 59-64
- [16] Rubanik Jr., V. V. Rubanik, V. V. Klubovich, V. V. (2008) The influence of ultrasound on the shape memory behavior, *MSE A* 481-482 620-622
- [17] Buchelnikov, V., Pikshtein, I., Grechishin, R., Khudoverdyan, T., Koledov, V., Kuzavko, Y., Nazarkin, I., Shavrov, V. Takagi, T. (2004) Ultrasound-induced martensitic transition in ferromagnetic Ni_{2.15}Mn_{0.81}Fe_{0.04}Ga shape memory alloy, *J. Magn. Mater.* 272-276 2025-2026
- [18] Steckmann, H., Kolomytsev, V. I., Kozlov, A. V. Acoustoplastic effect in the shape memory alloy Ni-Ti-Re at ultrasonic frequency, *Ultrasonics* 37 (1999) 59-62
- [19] Brezcko, T., Rubanik, V. V., Rubanik Jr., V. V. (1999) Study of behaviour NiTi-alloy under action of ultrasound, *Proc. of SPIE, NDTCS-98* 3687 310-312
- [20] Bao, M., Zhou, Q., Dong, W., Lou, X., Zhang, Y. (2013) Ultrasound-modulated shape memory and payload release effects in a biodegradable cylindrical rod made of chitosan-functionalized PLGA microsphere, *BioMac*
- [21] Goliboroda, I., Rusinko, K., & Tanaka, K. (1999) Description of a Fe-based shape memory alloy thermomechanical behavior in terms of the synthetic model. *Computational materials science*, 13(4), 218-226

- [22] Rusynko, K. M., & Shandrivskiy, A. H. (1996) Irreversible deformation in the course of a martensite transformation. *Materials Science*, 31(6), 786-789
- [23] Rusinko, A., & Rusinko, K. (2011) *Plasticity and creep of metals*. Springer Science & Business Media
- [24] Likhachov, V. A. and Malinin, V. G. (1993) *Structural-Analytic Theory of Elasticity* [in Russian] Nauka, St. Petersburg
- [25] <https://matthey.com/products-and-markets/other-markets/medical-components/resource-library/nitinol-technical-properties>
- [26] Bradley, D. (1965) Sound Propagation in Near-Stoichiometric Ti-Ni Alloys. *The Journal of the Acoustical Society of America*, 37(4), 700-702